JOURNAL OF MATERIALS SCIENCE: MATERIALS IN MEDICINE **16** (2005) 447–453

Incorporation of fluorine ions into hydroxyapatite by a pH cycling method

H. QU, A. L. VASILIEV, M. AINDOW, M. WEI*
Department of Materials Science and Engineering, Institute of Materials Science, University of Connecticut, Storrs, CT 06269-3136, USA
E-mail: m.wei@ims.uconn.edu

Fluorine ions were incorporated into hydroxyapatite (HA) using a pH cycling method and the resulting materials were studied using transmission electron microscopy (TEM), X-ray diffraction (XRD), and electrochemical analysis. TEM observations showed that fluoridated hydroxyapatite (FHA) nanoparticles with a narrow particle size distribution were obtained at several different levels of fluorine incorporation. Significant particle growth was observed following calcining at 1200 °C. The TEM data revealed that, instead of forming laminated structures, a mixture of HA and FA was obtained, and that this mixture transformed into a single homogeneous FHA phase upon heating. It was found that the efficiency of fluorine incorporation did not vary significantly with the initial HA particle size, but increased as the fluorine content of the initial solution was increased. A relatively low fluorine incorporation efficiency, ~60%, was attained for most of the FHA samples and this was attributed to the short holding time at each pH cycle and the limited number of pH cycles employed in the current study.

1. Introduction

It is well known that fluorine exists as a trace element in biological apatites [1]. Fluorine has also been used for the prevention of caries and the treatment of osteoporosis for several decades [2]. Recent studies have shown that low levels of fluorine can enhance bone formation *in vivo* [3, 4]. Thus, fluoridated hydroxyapatite $Ca_5(PO_4)_3(OH)_{1-x}F_x (0 < x < 1)$ (FHA), where F^- partially replaces OH^- in hydroxyapatite $Ca_5(PO_4)_3(OH)$ (HA), is potentially a very interesting biomaterial. HA is the main inorganic phase of human hard tissues and is widely used for bone substitutions or as repair material for bones and teeth [5]. It was suggested that fluorine tends to increase the stability and decrease the solubility of HA because the a-axis lattice parameter of FHA is smaller than that for HA [6, 7]. Thus, FHA exhibits a very attractive combination of stability and biocompatibility. However, it has been reported that if all of the OH^- groups in HA are replaced by F^- to form fluoroapatite $Ca_5(PO_4)_3F$ (FA), the resulting material is not osteo-conductive [8]. Moreover, the high F^- content might lead to severe adverse effects such as osteomalacia [9]. As a result, various methods have been developed in an attempt to tailor the fluorine content of FHA to achieve the best biological properties.

FHA can be either prepared using a solid-state reaction or a wet-chemical process, but the later is used more commonly. There are several different approaches used in wet-chemical processing of FHA. These include: combining the reactant agents in solution and precipitating FHA [10]; preparing HA, and obtaining FHA by F^-:OH^- ion exchange through a pH cycling process [11]; and using a multi-step fluorine supply system to form laminated FHA [12]. FHAs formed by these different approaches have been characterized using wet chemical analysis, X-ray diffraction (XRD), Fourier transform infra-red (FTIR) spectrometry, Raman infra-red spectrometry and nuclear magnetic resonance (NMR) spectrometry [6, 11–15]. Transmission electron microscopy (TEM) has also been used to reveal the small structural differences that occur with increasing fluorination in FHA precipitates [6, 11]. In this manner, Okazaki [6] demonstrated that a laminated structure is formed in micrometer sized FHA precipitates produced via a multi-step fluorine supply process.

In our previous work, nanoparticulate FHA samples with various fluorine contents were prepared successfully by a pH-cycling method and they were characterized using FTIR and XRD [16]. In this paper, we report a combined XRD and TEM study on the mechanisms of fluorine incorporation into these materials.

2. Methods

2.1. Synthesis of HA and FHA

The synthesis of HA involved a metathesis reaction which has been described in detail elsewhere [16]. Calcium nitrate (99%, Sigma) and di-ammonium

*Author to whom all correspondence should be addressed.

phosphate (99%, Sigma) solutions were prepared with a Ca/P ratio of 1.67, and the pH of each solution was brought up to 11-12 by adding NH_4OH (29.5%, Sigma). The phosphate solution was added to the calcium nitrate solution, resulting in the precipitation of HA. The precipitates were aged for 7 days at room temperature. They were then washed, dried and ground into a fine powder.

Six FHA samples with different fluorine contents were synthesized: these were designated FHA1, FHA2, FHA3, FHA4, FHA5, and FHA6. Firstly, sodium fluoride (100%, Sigma) was dissolved in 2 liter of distilled water to prepare solutions with concentrations of 2.5×10^{-3}, 5×10^{-3}, 7.5×10^{-3}, 1×10^{-2}, 1.25×10^{-2}, and 1.50×10^{-2} M, respectively. 10 g of the HA powder was suspended in each of the solutions and the solutions were equilibrated at pH 7 overnight. The pH of the solution was then brought down to 4 by slowly dropping 1 M HNO_3 (70%, Aldrich) into each solution. After 30 min, the pH of each solution was brought up to 7 again by adding 1 M NaOH (1 N standard solution, Acros). This pH cycling process was repeated three times. The resulting precipitates were then aged for one day at room temperature, dried and ground into fine powders.

2.2. Milling

Some of the HA powders were ball milled before soaking in sodium fluoride solution to study the effect of particle size on fluorine incorporation. The particle size of the HA powder before and after milling was measured using a submicron particle sizer (Autodilute model 370, NICOMP).

The milling process was carried out in a Teflon bottle with a ball-to-powder weight ratio of 15:1. After 20 h of milling, the HA powder was dried at 80 °C overnight. 10 g of this milled HA powder was soaked in 2 liter of a sodium fluoride (100%, Sigma) solution with a concentration of 1×10^{-2} M, i.e. the same as that used to prepare FHA4. After repeating this pH cycling process 3 times, the final dried powder was designated FHA4-M.

2.3. Calcination

HA, FHA1, FHA2, FHA3, and FHA4 specimens were calcined at three different temperatures, 1200, 1300, and 1400 °C. These temperatures were established by heating at a rate of 5 °C/min. The samples were held at the temperature for 1 h and then cooled to room temperature in the furnace at a rate of 5 °C/min.

2.4. XRD analysis

Portions of each of the calcined FHA powder samples were examined using XRD (BRUKER AXS D5005) with Ni-filtered Cu K_α radiation to detect the onset of decomposition. A step size of 0.02° and a scan speed of 1°/min were used.

2.5. Fluorine, calcium and phosphate measurements

Fluorine concentration measurements were performed using a F-selective electrode (Orion 94-09) in a total ionic strength adjustment buffer (TISAB). 0.2 g of each sample was dissolved in 10 ml 1 M nitric acid and then diluted with 200 ml distilled water. The fluorine content was determined by mixing 10 ml of this solution with 10 ml of the buffer. Standard solutions made from NaF were used to calibrate the measurement with the same buffer solution. The efficiency of F-incorporation into the HA was then calculated from these data.

The calcium and phosphorous analyses of FHA1, FHA2, FHA3, and FHA4 were conducted by inductively-coupled plasma optical emission spectrometry (ICP-OES-Trace Scan Advantage, Thermo-Jarrel Ash), and the Ca/P and F/Ca ratios were calculated.

2.6. TEM observation and electron diffraction and EDX analyses

TEM analyses were conducted on the uncalcined samples and those calcined at 1200 °C. For each of the powders a few mg were dispersed in alcohol by sonicating for two hours. The resulting dilute suspensions were deposited onto copper TEM grids coated with a thin Formvar-carbon support film, and allowed to air-dry. Preliminary microstructural analyses were performed in a Philips EM-420 TEM equipped with a Kevex-Noran Be-window EDXS system, and operating at an accelerating voltage of 100 kV. This instrument was used to obtain conventional images and selected-area electron diffraction (SAED) patterns from the FHA powder particles before and after calcination. For some of the uncalcined FHA samples, high resolution TEM lattice images were obtained in a JEOL JEM-2010 TEM equipped with an ultra-high resolution objective lens pole-piece (spherical aberration coefficient $C_s \approx 0.5$ mm) and operating at an accelerating voltage of 200 kV. In this configuration, the point-to-point resolution at Scherzer defocus was <0.19 nm. This instrument is also equipped with an atmospheric thin window EDXS system (EDAX Phoenix), which was used to obtain chemical microanalysis from clusters of FHA particles.

3. Results

3.1. Fluorine content and particle size

The F contents measured from each of the uncalcined FHA samples are shown in Table I together with the calculated efficiency of F^- incorporation. For FHA1,

TABLE I Effect of fluorine content on the efficiency of fluorine incorporation

Sample	F- added to the initial solution (mol F^-/ mol apatite)	F^- incorporated (mol F/mol apatite)	Efficiency of F-incorporation (%)
FHA1	0.25	0.232	92.8
FHA2	0.50	0.314	62.8
FHA3	0.75	0.425	56.7
FHA4	1.0	0.569	56.9
FHA5	1.25	0.834	66.7
FHA6	1.50	0.952	63.5
FHA4-M	1.00	0.579	57.9

TABLE II Molar ratios of Ca/P and F/Ca measured by different techniques

Measuring technique	Molar ratio	HA	FHA1	FHA2	FHA3	FHA4
ICP	Ca/P	1.65	1.65	1.65	1.67	1.68
F-electrode	F/Ca	0	0.049	0.064	0.091	0.115

the efficiency is very high at ≈93%, whereas for the other samples the efficiency is around 60% in each case. As such, the variation of F^- content for these other samples with the concentration in the initial solution is approximately linear.

SEM micrographs obtained from each of the unmilled samples revealed that the particles formed agglomerates with mean diameters of 1.5–2.4 μm. There was no measureable effect of agglomerate size upon F^- incorporation and this is shown most clearly by a comparison of samples FHA4 and FHA4-M. For the unmilled sample (FHA4) the mean agglomerate size was 2.1 μm whereas for the milled sample this was reduced to 0.7 μm. Although the agglomerate sizes differ by a factor of 3, the F^- contents and incorporation efficiencies for the two samples are almost identical. A comparison of the Ca/P and Ca/F ratios for each sample as measured by ICP-OES and F-electrode techniques is presented in Table II.

3.2. Decomposition analysis by XRD

XRD was used to determine the phase distribution for calcined samples of HA and each of the FHA powders. Examples of these data are presented in Figs. 1, 2 and 3. It was found that the variation of phase distribution with calcination temperature was sensitive to the fluorine content. For pure HA, only the apatite peaks are observed after calcining at 1200 °C (Fig. 1(a)), and indeed these peaks were observed for all of the FHA samples processed at this temperature (e.g. Fig. 2(a)). When the calcining temperature was increased to 1300 °C, both HA and FHA1 samples were partially decomposed to β-tricalcium phosphate (β-TCP) (Figs. 1(b) and 2(b)), but no evidence for this was observed in FHA2, FHA3, and FHA4. At 1400 °C, more β-TCP was detected in both HA and FHA1 than in those calcined at 1300 °C (Figs. 1(c) and 2(c)), while FHA2, FHA3 and FHA4 were still not decomposed (Fig. 3). Moreover, it was found that more β-TCP was detected in HA than in FHA1 at both 1300 and 1400 °C, which confirmed that the thermal stability of FHA increased with the fluorine-content in the specimens.

3.3. TEM observations

TEM images obtained from samples of the as-synthesized powders revealed that the morphology of the powder particles was highly uniform consisting of rods with an aspect ratio of between 2 and 5. These particles were also extremely fine with mean dimensions of approximately 60 nm in length, and 15 nm in width in each case. Not only are these HA and FHA particles significantly smaller than those reported elsewhere in the literature, but also they are more monodisperse. Representative images obtained from samples HA, FHA1,

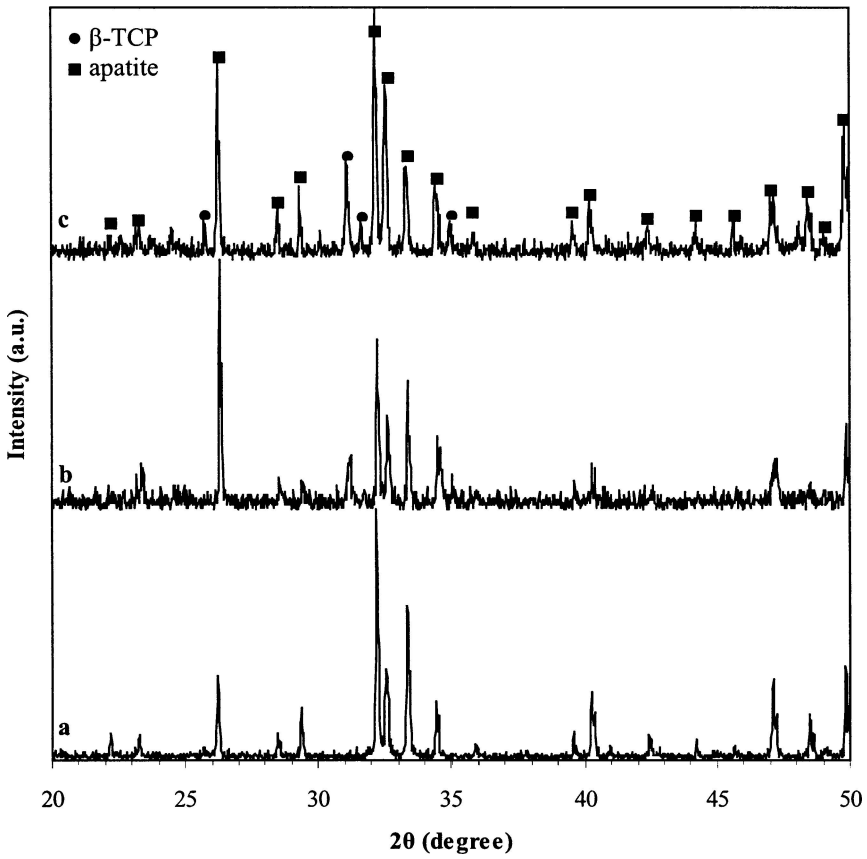

Figure 1 XRD patterns of FHA0 calcined at (a) 1200, (b) 1300, and (c) 1400 °C.

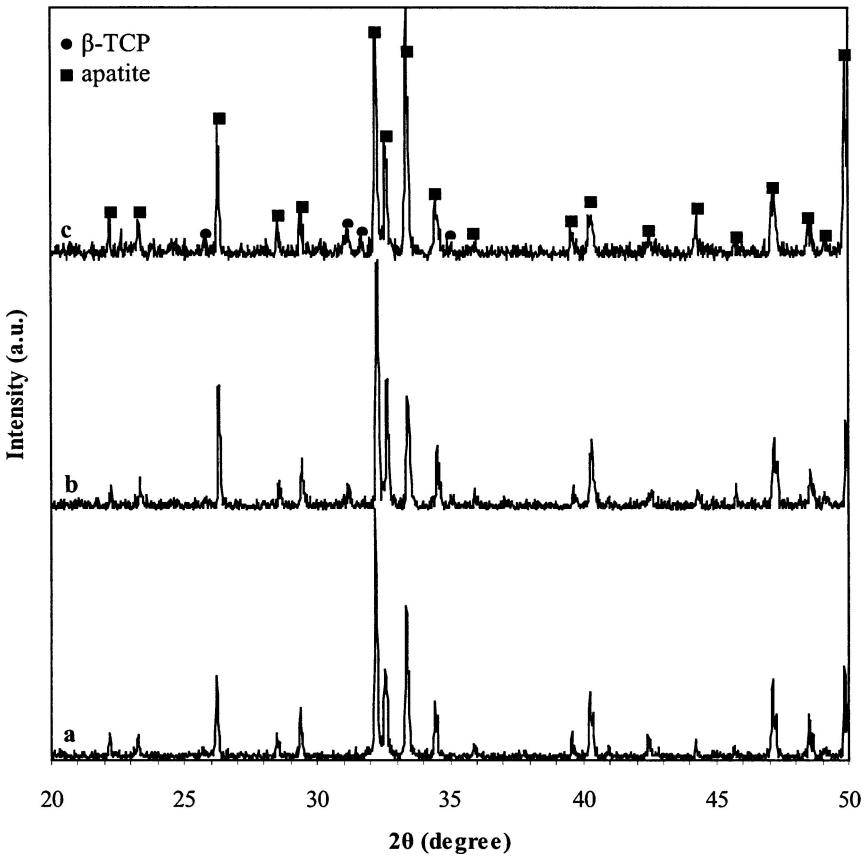

Figure 2 XRD patterns of FHA1 calcined at (a) 1200, (b) 1300, and (c) 1400 °C.

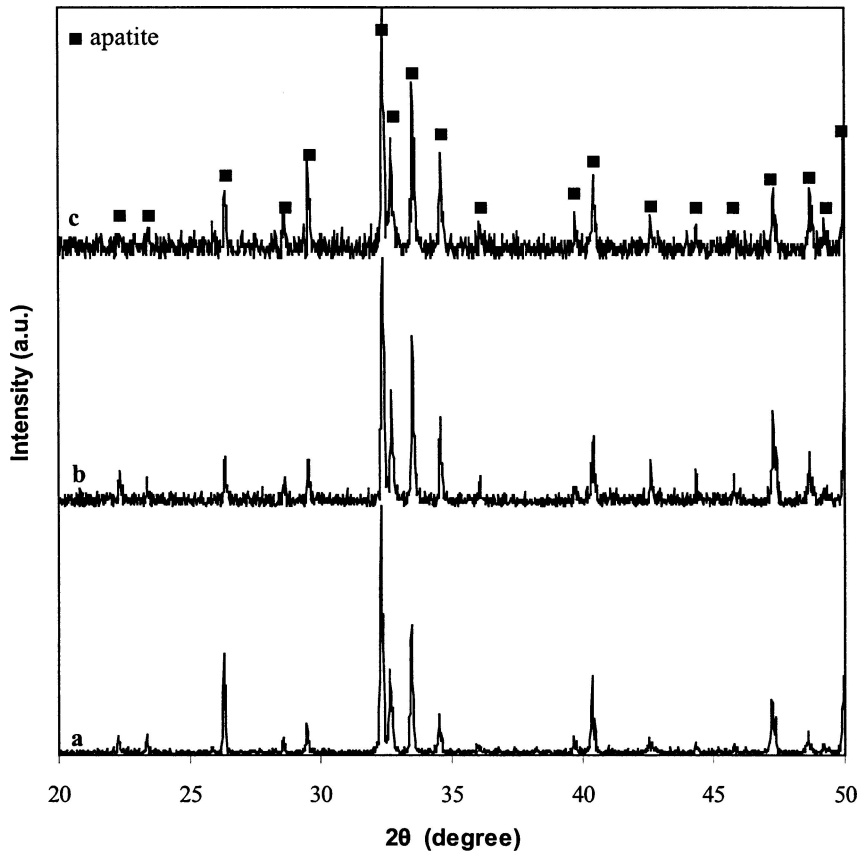

Figure 3 XRD patterns of (a) FHA2, (b) FHA3, (c) FHA4 calcined at 1400 °C.

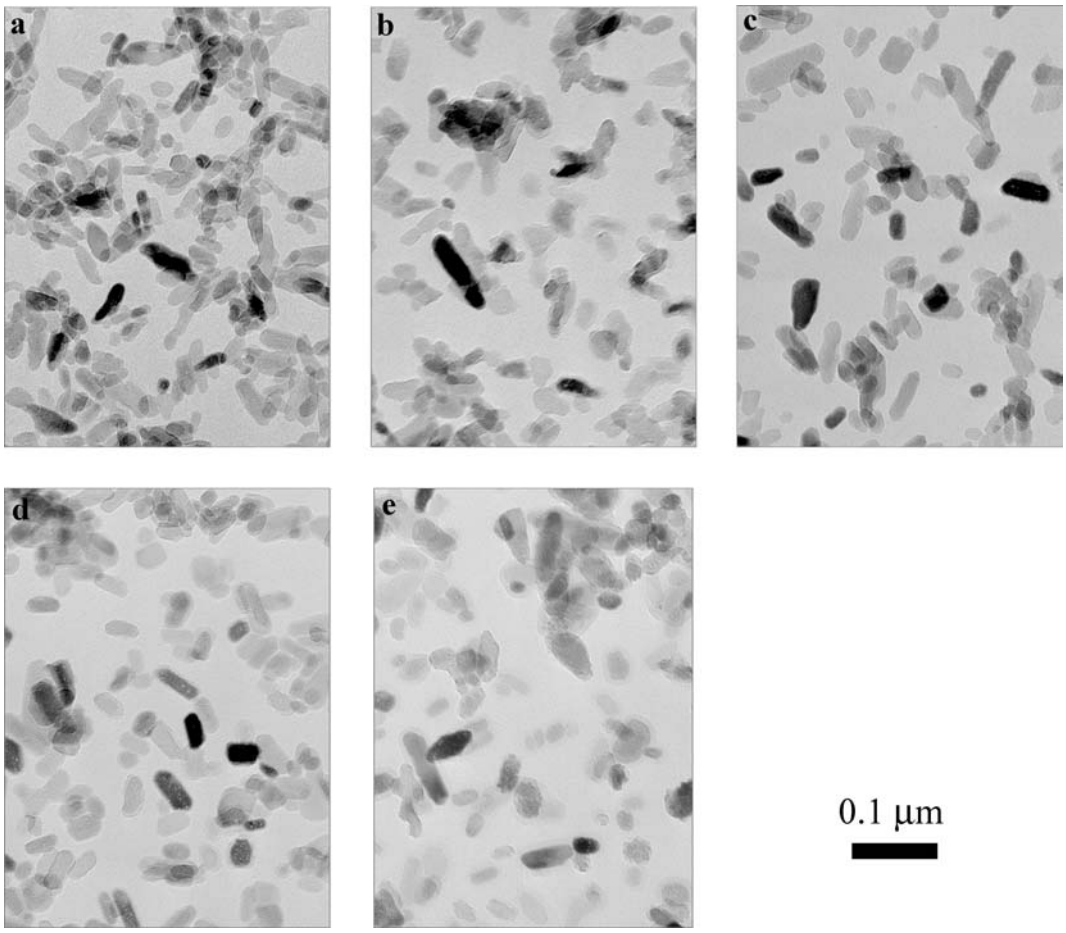

Figure 4 TEM images of uncalcined (a) HA, (b) FHA1, (c) FHA2, (d) FHA3 and (e) FHA4.

FHA2, FHA3, and FHA4 are shown in Fig. 4. Similar images were also obtained for FHA5 and FHA6.

Electron diffraction data obtained from these samples were consistent with XRD data reported previously for the same samples. A typical SAED pattern obtained from the FHA4 sample is shown in Fig 5. In this and similar patterns obtained from the FHA samples, all of the rings could be identified as arising from FA (PDF 15-876) or HA (PDF 9-432). We note, however that in some cases it was difficult to distinguish the two because the only major distinction between these structures is a subtle difference in lattice parameters.

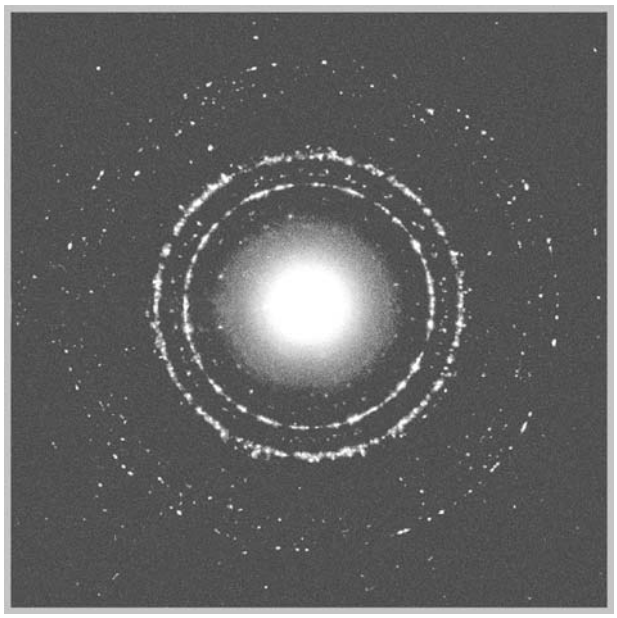

Figure 5 Electron diffraction pattern of uncalcined HA particle clusters.

High resolution TEM lattice images obtained from individual powder particles indicated that these are all uniform single crystals. Two such images are shown in Fig. 6, one each from HA and FHA4, although we note that very similar images were obtained from other samples. Fig. 6(a) shows one end of a HA particle oriented with the beam direction, **B**, parallel to $[11\bar{2}0]$. The image contains pronounced $1\bar{1}00$ and 0002 lattice fringes oriented parallel and perpendicular to the major axis of the particle, respectively. As such, the major axis of the particles is parallel to [0001] and this is consistent with the analyses of other images obtained from this and the FHA samples. A second example is shown in Fig. 6(b) which is a lattice image obtained from one end of a FHA4 particle with **B** // $[1\bar{1}00]$. In this case the image contains $11\bar{2}0$ and 0002 lattice fringes oriented parallel and perpendicular to the major axis of the particle, respectively.

After calcining, much larger FHA particles were observed and one example is shown in Fig. 7. These particles were frequently polycrystalline and contained individual grains of up to 0.5 μm in diameter. Although the grain morphology varied somewhat, occasional grains exhibited a morphology reminiscent of the original nanoparticles and with the same crystallographic

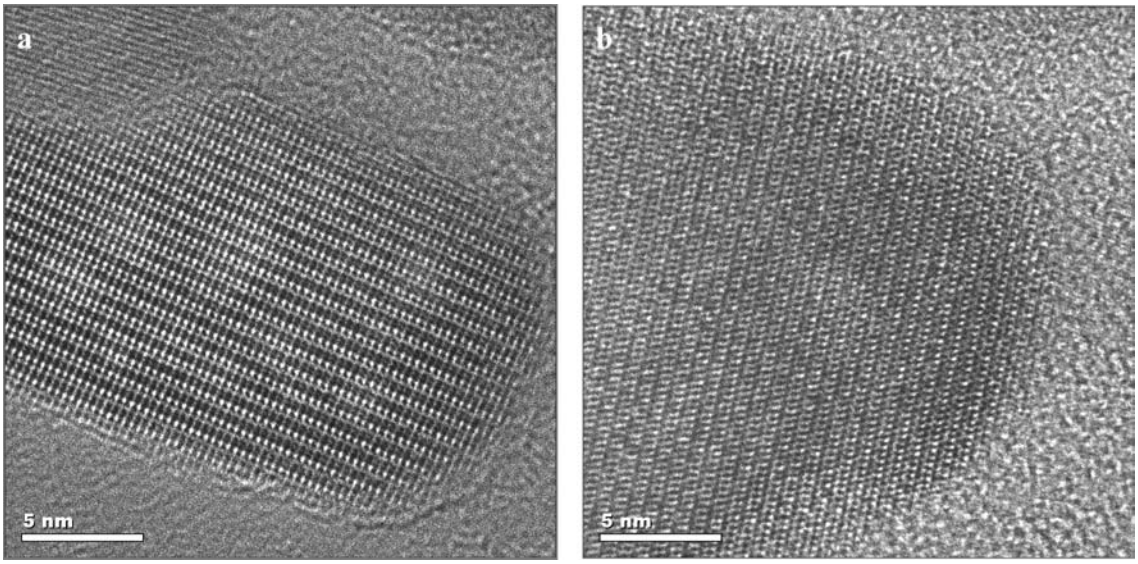

Figure 6 High resolution TEM images of uncalcined of (a) HA and (b) FHA4.

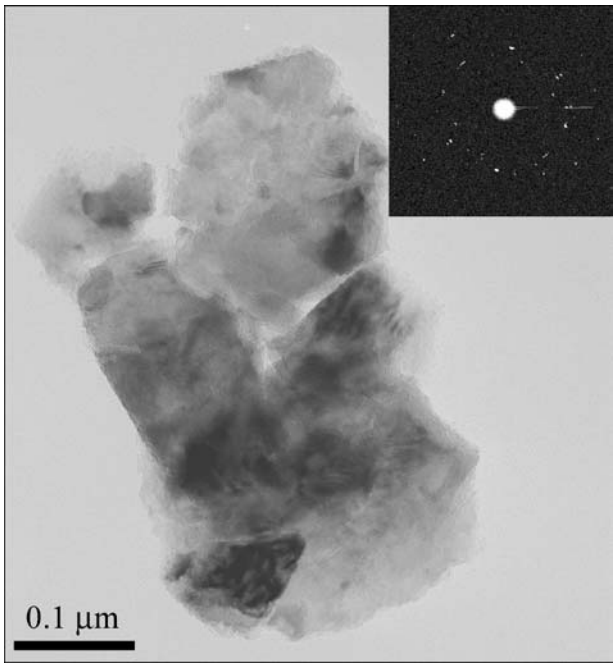

Figure 7 TEM image of calcined FHA4 particles.

directions parallel and perpendicular to the boundaries. One example of such a grain can be found on the lower left of the particle in Fig. 7.

4. Discussion

When the HA powder was soaked in the NaF solution, FHA was formed through ionexchange between F^- and OH^- [17, 18]. Duff *et al.* [19] calculated the thermodynamic activity of this system (FHA, HA and fluoride solution) and found that when the pH of the fluoride solution was at 4.0, more HA dissolved into the solution, reacted with F^- ions, and formed calcium fluoride. The calcium fluoride then reacted with the other ions in the solution and formed FHA as the pH increased to 7.0. The cumulative effect of these two-step pH fluctuations can be expressed by the following equation:

$$Ca_5(PO_4)_3OH + xF^- + xH^+ \rightarrow Ca_5(PO_4)_3F_x(OH)_{1-x} + xH_2O \quad (1)$$

The rate of FHA formation can be written as:

$$\frac{d(FHA)}{dt} = kC_{F^-}^x C_{H^+}^x \quad (0 < x < 1) \quad (2)$$

where d(FHA)/dt is the rate of FHA formation, k is the rate constants for FHA formation, C_{F^-} and C_{H^+} are F^- and H^+ concentrations in the solution, respectively. Apparently, the higher the fluorine in the solution, the higher the rate of FHA formation.

As the FHA precipitates are F-rich (i.e. $x \approx 1$) after integration, Equation (2) can be written as:

$$C_{F_e^-} = C_{F_0^-} e^{-Kt} \quad (3)$$

where the $K = kC_{H^+}$, $C_{F_e^-}$ is the fluorine concentration remaining in the solution, and $C_{F_0^-}$ is the fluorine concentration added to the initial solution. This indicates that the longer the residence time (t) at each pH cycle, the higher the efficiency of fluorine incorporation.

Unfortunately, the rate of this F:OH exchange process is very slow. Duff *et al*. reported that it took 10 days, five pH cycles, and a slight excess of fluorine ions to have the F^- totally replace the OH^- groups in HA and form $Ca_5(PO_4)_3F$ [19]. In contrast, the samples in the current study were only held for 30 min in each pH cycle, and only three pH cycles were performed. As a result, the efficiency of fluorine incorporation was much lower than the value of 95% reported by Duff *et al*. [19]. Only FHA1 approached this value in the present work. For all of the other samples, the efficiency was approximately 60% (Table I). Reducing the agglomerate size of HA (FHA4-M) did not improve the fluorine incorporation as the fluorine concentration in the solution was unchanged.

The structure of FHA particles was also studied. Okazaki *et al.* [6] used a wet-chemical process in which $Ca(CH_3COO)_2 \cdot H_2O$ and $NH_4H_2PO_4$ were converted to fluoridated HA particles with an average size of approximately 5 μm. It was reported that these apatite particles demonstrated a laminated structure with either HA covered with FA (H-FAp apatite) or *vice-versa* (i.e. F-HAp apatite). In contrast, the FHA particles formed using the pH cycling method were nanometer-sized and showed no evidence for internal phase separation in either conventional bright field TEM images (Fig. 4) or in high-resolution lattice images (Fig. 6). Some evidence for phase separation was observed in electron diffraction patterns obtained from such samples. This suggests that the powder samples consist of a mixture of HA and FA (i.e. fully substituted FHA). The only way in which one can reconcile these apparently contradictory conclusions is if the uncalcined FHA powders were to consist of a mixture of HA (unsubstituted) and FA (fully substituted) particles.

Our previous FTIR and XRD data on these samples support this interpretation [16]. The OH band was detected in FTIR spectra obtained from all of the uncalcined FHA specimens, indicating the presence of HA. Moreover, XRD patterns obtained from all the uncalcined FHA samples showed the same systematic shift of the 211, 112 and 300 peaks to higher 2θ values (i.e. smaller d-spacings) than those for HA. The form of these peaks, however, indicated that these are a convolution of the peaks from HA and FA. This could explain the insensitivity of the peak positions to F^- content since only the proportions of the two phases would change, not the lattice parameters. This is in stark contrast to the data reported by Okazaki *et al*. [6, 12] who observed a progressive shift in the positions of the 211 and 300 peaks of FHA with increasing F content.

After calcination, the FHA particles were much larger and were polycrystalline (Fig. 7). Interdiffusion of F^- and OH-ions had occurred resulting in homogenous FHA. Here again this is supported by the FTIR and XRD results from our previous study [16]. It was found that the OH band at 630 cm^{-1} was not present in any of the FTIR spectra from the calcined specimens due to the absence of HA, while the shift of the 211, 112 and 300 peaks to higher angles varied systematically with increasing fluorine content.

The decomposition studies are also consistent with this transformation sequence. It was found that pure HA decomposed at 1300 °C, whereas FHA1 and FHA2 decomposed at 1400 °C, and the rest of the FHA specimens did not decompose at the temperatures used in this study. This also indicates that a homogenous FHA had formed on calcination since for a mixture of FA and HA, one would expect the onset of decomposition at 1300 °C, as observed pure HA.

5. Conclusions

Nano-sized FHA particles with various fluorine contents were obtained through a pH cycling method. The mechanisms by which fluorine ions are incorporated into HA were studied. For most of the samples, a low fluorine incorporation rate of approximately 60% was achieved due to the short residence time in each pH cycle and the limited number of cycles used. Data from TEM, XRD and FTIR indicate that pH cycling produces a mixture of FA and HA particles instead of the laminated structure reported previously. Upon calcining, chemically homogeneous FHA polycrystals are formed with grain sizes an order of magnitude larger than the uncalcined particles.

Acknowledgments

The authors would like to thank Prof. Pedro Cid-Aguero for his assistance with fluorine analysis, and Prof. R.Z. LeGeros for her assistance with Ca and P measurements. Mei Wei also gratefully acknowledges the support of K.C. Wong Education Foundation, Hong Kong.

References

1. A. E. W. MILES, in "Structure and Chemical Organization of Teeth" (Academic Press, New York, 1967) Vol 1.
2. J. R. MELLBERG and L. W. RIPA, in "Fluoride in Preventive Dentistry: Theory and Clinical Applications" (Quintessence Publishing Co. Inc., Chicago, 1983).
3. M. SUNDFELDT, M. WIDMARK, A. WENNERBERG, J. KÄRRHOLM, C. JOHANSSON and L. CARLSSON, *J. Mater. Sci. Mater. Med.* **13** (2002) 1037.
4. M. SUNDFELDT, J. PERSSON, J. SWANPALMER, A. WENNERBERG, J. KÄRRHOLM, C. B. JOHANSSON and L. V. CARLSSON, *ibid.* **13** (2002) 1045.
5. E. C. SHORS and R. E. HOLMES, in "An Introduction to Bioceramics," edited by L. L. Hench and J. Wilson (World Scientific, Singapore, 1993).
6. M. OKAZAKI, Y. MIAKE, H. TOHDA, T. YANAGISAWA, T. MATSUMOTO and J. TAKAHASHI, *Biomaterials* **20** (1999) 1421.
7. M. WEI, J. H. EVANS, T. BOSTROM and L. GRØNDAHL, *J. Mater. Sci. Mater. Med.* **14** (2003) 311.
8. E. LUGSCHEIDER, M. KNEPPER, B. HEIMBERG, A. DEKKER and C. KIRKPATRICK, *ibid.* **5** (1994) 371.
9. K. W. LAU, K. ÅKESSON, C. R. LIBANATI and D. J. BAYLINK, in "Anabolic Treatments for Osteoporosis," edited by J. F. Whitfield and P. Morley (CRC Press; 1997).
10. L. J. JHA, S. M. BEST, J. C. KNOWLES, I. REHMAN and J. D. SANTOS, *J. Mater. Sci. Mater. Med.* **8** (1997) 185.
11. E. J. DUFF, *Engl. Chem. Ind.* **8** (1974) 349.
12. M. OKAZAKI, H. TOHDA, T. YANAGISAWA, M. TAIRA and J. TAKAHASHI, *Biomaterials* **19** (1998) 919.
13. G. PENEL, G. LEROY, C. REY, B. SOMBRET, J. P HUVENNE and E. BRES, *J. Mater. Sci. Mater. Med.* **8** (1997) 271.
14. M. BRAUN, P. HARTMANN and C. JANA, *ibid.* **6** (1995) 150.
15. M. OKAZAKI, *Biomaterials* **16** (1995) 703.
16. H. QU and M. WEI, *J. Mater. Sci. Mater. Med.* **16** (2005) 129.
17. L. M. RODRÍGUEZ-LORENZO and K. A. GROSS, *J. Mater. Sci. Mater. Med.* **14** (2003) 939.
18. S. CHANDER, C. C. CHIAO and D. W. FUERSTENAU, *J. Dent. Res.* **61** (1982) 403.
19. A. C. RAMSEY, E. J. DUFF, L. PATERSON and J. L. STUART, *Caries Res.* **7** (1973) 231.

Received 1 July
and accepted 1 November 2004